

A&A manuscript no.
(will be inserted by hand later)

Your thesaurus codes are:
06 (11.01.2; 11.01.2; 11.09.1; 11.19.1; 13.25.2)

The Warm Absorber constrained by the coronal lines in Seyfert 1 galaxies

D. Porquet¹, A.-M. Dumont¹, S. Collin¹, and M. Mouchet^{1,2}

¹ DAEC, Observatoire de Paris, Section Meudon, F-92195 Meudon Cedex, France

² Université Denis Diderot, F-75251 Paris Cedex 05, France

Received ; accepted

Abstract. We present results of the photoionization code IRIS, which calculates the spectrum emitted by the Warm Absorber (WA) in Seyfert 1 galaxies for a large grid of parameters (density, column density, ionization parameter...). We show that in Seyfert 1s, coronal lines ([Fe X], [Fe XI], [Fe XIV]...), whose emission region shares common characteristics with the WA, could be formed in the WA. Unlike the absorption edges, such as those of O VII and O VIII observed in soft X-rays which are produced by the WA, these lines strongly constrain the physical parameters of the WA, especially the hydrogen density. Indeed, in order to avoid producing coronal line equivalent widths larger than observed, a high density ($n_H \geq 10^{10} \text{ cm}^{-3}$) is required for the WA in most cases. This result is obtained for the mean observed Seyfert 1 features, as well as for the case study of MCG-6-30-15. It implies that the distance of the WA from the incident radiation source is of the order of that of the Broad Line Region (BLR).

Key words: Galaxies: active – Galaxies: Seyfert – Galaxies: individual (MCG-6-30-15) – X-rays: galaxies – line: formation

1. Introduction

The Warm Absorber (WA) is an optically thin ionized medium, first proposed by Halpern (1984) in order to explain the shape of the X-ray spectrum of the QSO MR2251-178 observed with the Einstein Observatory. The main signatures of this medium are the two high-ionization oxygen absorption edges, O VII and O VIII at 0.74 keV and 0.87 keV respectively, seen in about fifty percent of Seyfert 1 galaxies (Nandra & Pounds 1994; Reynolds 1997, hereafter referred as R97).

Mihara et al. (1994) found with ASCA observations of NGC 4051 that the absorption edges of O VII and O VIII may be blueshifted by about 3%. This could be due to an

outflow velocity of $\sim 10\,000 \text{ km.s}^{-1}$.

According to Netzer (1993), an emission line spectrum from the WA should also be observed. Indeed, an O VII line (0.57 keV) was detected in NGC 3783 (George et al. 1995). Other Seyferts may also show oxygen emission lines: MCG-6-30-15 (O VII-O VIII: Otani et al. 1996 but the authors mentioned that those features could have an instrumental origin), and 1E 1615+061 (O VII-O VIII: Piro et al. 1997). The WA may also contribute to the emission of the UV lines (Shields et al. 1995, Netzer 1996), like Ne VIII 774Å (Hamann et al. 1995) and O VI 1034Å which are also produced in highly ionized regions.

The WA is generally thought to be a photoionized medium which lies on the line of sight of the ionizing X-ray source. But the possibility of collisional ionization is not ruled out, and it is therefore also investigated in this article.

In Seyfert 1 spectra, coronal lines are also observed. They are fine structure transitions in the ground level of highly ionized ions which have threshold energies above 100 eV. According to Penston et al. (1984), [Fe X] 6375Å is found in half Seyfert objects (with no preference between type-1 and type-2 Seyferts). From their Table 4, [Fe XI] 7892Å is detected in 6 of their 19 Seyfert 1s. In the sample used by Erkens et al. (1997) (hereafter referred as E97), the mean widths of the forbidden high ionization lines (FHILs) are intermediate between those of the Broad Line Region (BLR) and the Narrow Line Region (NLR), but in some cases the wings of the FHILs could be comparable to or broader than the BLR profiles. The FHIL region seems therefore to be located near the BLR, or between the BLR and the NLR. According to E97, it is located outside the BLR if the Unified Scheme is correct, since broad FHILs are also found in Seyfert 2 spectra. E97 confirmed that FHILs like [Fe X] 6375Å, [Fe XI] 7892Å and [Fe XIV] 5303Å are in average broader and more blueshifted than lower ionization lines like [Ne V] 3426Å and [Fe VII] 6087Å. The line widths and blueshifts are correlated with the ionization potential; In other words, the more ionized species have the larger

Send offprint requests to: D.Porquet

Correspondence to: Delphine.Porquet@obspm.fr

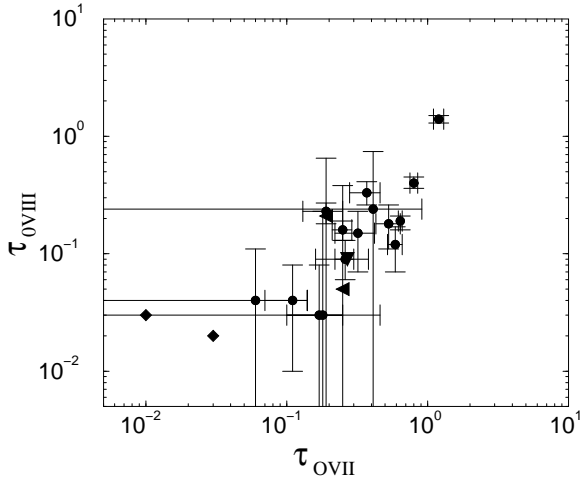


Fig. 1. $\tau_{\text{O VIII}}$ versus $\tau_{\text{O VII}}$ for 20 Seyfert 1s taken from Reynolds (1997). *Filled circle*: real value, *triangle left*: upper limit for $\tau_{\text{O VII}}$, *triangle down*: upper limit for $\tau_{\text{O VIII}}$ and *diamond*: upper limit for both values.

outflowing velocities.

Therefore, the WA and the high-ionization coronal line region seem to have common characteristics: a high ionization state, a location between the NLR and the BLR, and an outflowing gas.

This leads us to discuss the possibility that the coronal lines and the WA features could be produced in the same medium. We shall study the constraints that the coronal line intensities impose on the WA. Preliminary results have been already presented by Porquet & Dumont (1998).

In Sect. 2, we report the observational data relative to the coronal lines, to the optical depths of O VII and O VIII, and to the UV resonance emission lines. In Sect. 3, we discuss previous models and describe our computations. The results of a pure photoionized model and of an hybrid model (photoionized medium out of thermal equilibrium) for two shapes of incident continua are given in Sect. 4 and compared to the mean observed Seyfert 1 features. The particular case of MCG-6-30-15 is treated in Sect. 5. In Sect. 6, we discuss some implications of the results.

Throughout this article, we assume $H_o=50 \text{ km s}^{-1} \text{ Mpc}^{-1}$ and $q_o=0$.

2. Observational data

For Figures 1 to 5, when they exist, error bars are reported.

2.1. Optical depths of Oxygen

All the optical depth values at the O VII edge ($\tau_{\text{O VII}}$) and O VIII edge ($\tau_{\text{O VIII}}$) for Seyfert 1s are taken from R97, in

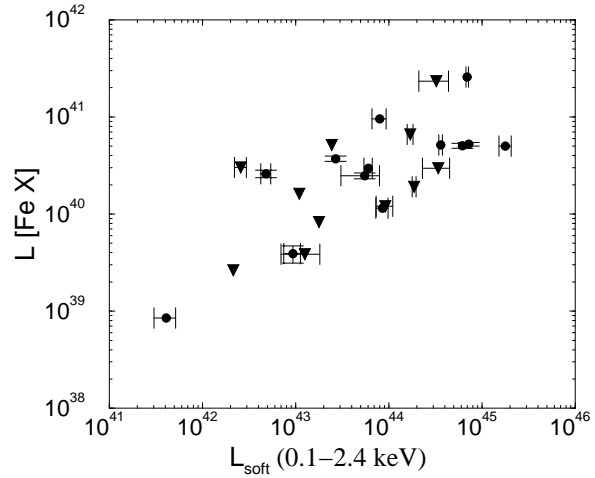


Fig. 2. Observed dereddened luminosity of [Fe X] (erg.s^{-1}) versus the soft X-ray luminosity (erg.s^{-1}). *Filled triangle down*: upper limit for [Fe X] and *filled circle*: real value. [Fe X] data are from Reynolds et al. (1997) (MCG-6-30-15), Penston et al. (1984) (NGC 7469, NGC 4051, NGC 5548, NGC 3516, Mrk 335, Mrk 509, IC 4329A, Fairall 9, Mrk 79, ESO G141-55, NGC 6814, IZw1, Mrk 618, Mrk 926), E97 (Mrk 9, Mrk 704, Mrk 1239, Akn 120, Akn 564), Morris & Ward (1988) (NGC 4593, Mrk 1347, Fairall 51, UGC 10683B, but line has not been corrected for blending with [O I] 6364Å). The soft X-ray luminosities are from Rush et al. (1996) (MCG-6-30-15, NGC 7469, NGC 4051, NGC 5548, NGC 3516, Mrk 335, Mrk 509, NGC 4593, IC 4329A, Mrk 704, Mrk 79, Mrk 1239, ESO G141-55, IZw1, Mrk 618), Schartel et al. (1997) (Fairall 9, Mrk 926), Boller et al. (1992) (Mrk 9, Akn 120, Akn 564, NGC 6814, Mrk 1347, Fairall 51, UGC 10683B).

order to have a homogeneous measurement sample. They have been derived using the same type of fit for all spectra. Figure 1 displays $\tau_{\text{O VII}}$ versus $\tau_{\text{O VIII}}$. There is a good correlation between the two parameters and $\tau_{\text{O VII}}$ seems to be almost always greater than $\tau_{\text{O VIII}}$. In some cases, variability of the optical depths is observed (as for example MCG-6-30-15: Reynolds et al. 1995 and NGC 4051: Guainazzi et al. 1996) and their position in this graph will change with respect to the Reynolds (1997) values.

In order to take into account the upper limits, we have calculated the mean value for the 20 objects in R97, using the Kaplan-Meier estimator with ASURV Rev 1.2 (Lavalley et al. 1992), which implements the method presented in Feigelson & Nelson (1985). We obtain $\tau_{\text{O VII}}=0.33\pm 0.07$ and $\tau_{\text{O VIII}}=0.20\pm 0.07$.

2.2. Coronal lines

Figure 2 displays dereddened [Fe X] 6375Å luminosity versus soft X-ray luminosity integrated over 0.1-2.4 keV. The values have been compiled in the literature (see Ref.

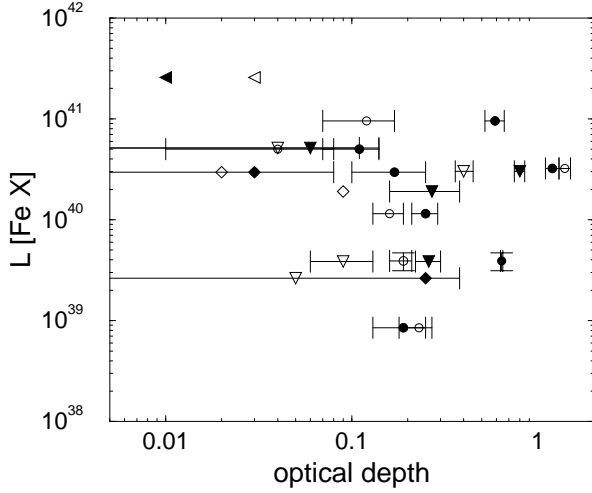


Fig. 3. Observed dereddened [Fe X] luminosity (erg.s^{-1}) versus $\tau_{\text{O VII}}$ and $\tau_{\text{O VIII}}$. *Filled symbols*: $\tau_{\text{O VII}}$ and *open symbols*: $\tau_{\text{O VIII}}$; *Triangle down*: upper limit for the Y-axis value (here the [Fe X] luminosity), *triangle left*: upper limit for the X-axis value and *diamond*: upper limits for both X and Y axis values.

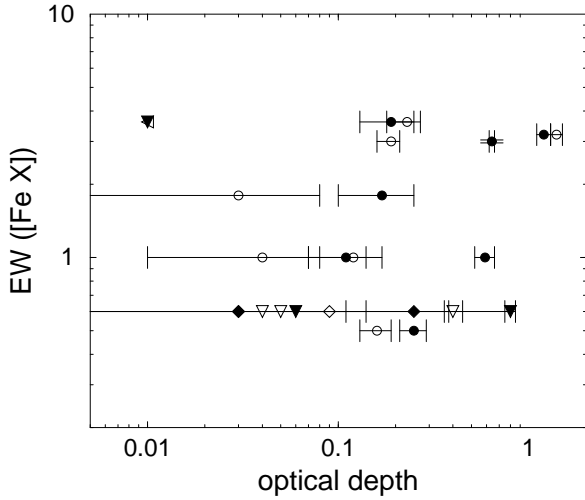


Fig. 4. Equivalent widths (in \AA) of [Fe X] versus the optical depths of O VII and O VIII. Same legend as Fig. 3.

in Fig.2 caption). There is a clear correlation between the two quantities, as also found by E97. This could be an indication that the high-ionization coronal lines, as the features of the WA, are formed either in a photoionized medium or in a medium which is partly photoionized and partly ionized by collisions. Figure 3 displays the observed dereddened luminosity of [Fe X] versus $\tau_{\text{O VII}}$ and $\tau_{\text{O VIII}}$. Figure 4 displays the [Fe X] equivalent width (EW) versus oxygen optical depths. No correlations between these quantities are apparent. We have calculated (same method as defined above) a mean [Fe X] equivalent width of $1.44 \pm 0.30 \text{ \AA}$. We take throughout this article

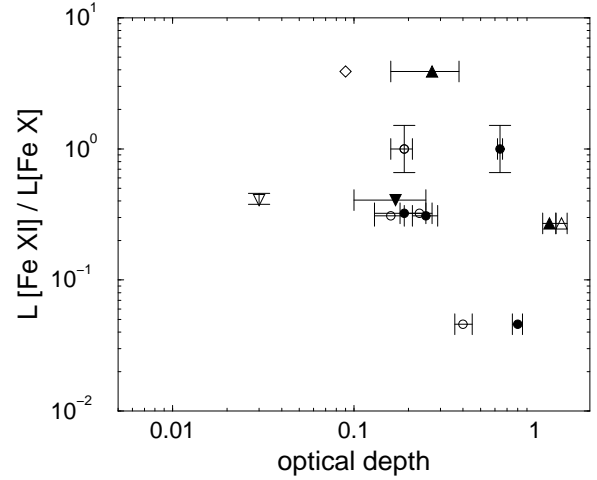


Fig. 5. Ratio of the observed dereddened luminosities of [Fe XI] over [Fe X] versus $\tau_{\text{O VII}}$ and $\tau_{\text{O VIII}}$. Same legend as Fig. 3 and *triangle up*: lower limit for the Y-axis value. [Fe XI] data are from Reynolds et al. (1997) (MCG-6-30-15), Penston et al. (1984) (NGC 7469, Mrk 79, NGC 4051, NGC 5548, NGC 3516, Mrk 335), and E97 (Mrk 9, Mrk 704, Mrk 705, Mrk 1239, Akn 120, Mrk 699, Akn 564).

$\text{EW}[\text{Fe X}] = 1.5 \text{ \AA}$.

For [Fe XI] 7892 \AA , we obtained a mean EW of about 4 \AA with only 3 EWs available for MCG-6-30-15, NGC 3783 and Mrk 1347 (Morris & Ward 1988). Figure 5 displays the luminosity ratio [Fe XI]/[Fe X] versus optical depths of O VII and O VIII. For the reported objects, the [Fe X] luminosity is greater than the [Fe XI] luminosity, except for one object.

For [Fe XIV] 5303 \AA , E97, who have selected objects in which the presence of FHILs has already been reported in the literature, found that only 4 of their 15 objects ($\sim 27\%$) required the presence of a significant [Fe XIV] contribution. So this line is generally not detected in Seyfert 1s. The resolution and S/N of their spectra were not sufficient to separate the blend of [Fe XIV] 5303 \AA + [Ca V] 5309 \AA and no [Fe XIV] EW values are quoted. Since only one spectrum has been plotted, we are thus unable to determine mean values for this coronal line. Nevertheless when [Fe XIV] is present, its flux is significant ($>25\%$ of the [Ca V] flux), then we will use $\text{EW}[\text{Fe XIV}] = 3 \text{ \AA}$ as a conservative upper limit. We will also use a value of 2 \AA to illustrate the sensitivity of this EW value on the physical parameters.

Until now, only very little information concerning some infrared coronal lines has been published for Seyfert 1s: for NGC 7469 ([Si X] 1.43 μm and [S XI] 1.93 μm : Thompson 1996, [Fe XII] 2.20 μm : Genzel et al. 1995) and for NGC 3516 ([Ca VIII] 2.32 μm : Giannuzzo et al. 1995). Mean EWs for these coronal lines cannot be determined. We will as-

sume that they are smaller than 10 \AA , which is compatible with the data of NGC 3516.

2.3. UV high-ionization resonance lines: O VI 1034Å and Ne VIII 774Å

Resonance lines correspond to allowed transitions to the ground level. Zheng et al. (1997) who have constructed a composite Radio-Quiet quasar spectrum with 101 quasars with $z > 0.33$ gave: $\text{EW}(\text{Ne VIII}) = 4 \text{ \AA}$. According to Figure 2 of Zheng et al. (1995), the $\text{EW}(\text{O VI})$ for a sample of 24 Radio-Quiet Quasars is about 7 \AA (the four atypical EWs $>> 20 \text{ \AA}$ being excluded).

3. Calculations

3.1. Previous models

The WA has been investigated by Netzer (1993, 1996). In his photoionization code "ION", he considered not only the absorption properties but also the emission and reflection spectra, which were not included in previous computations. He showed that intense X-ray lines as well as a non negligible reflection continuum might be produced. So the spectral shape could be changed significantly with respect to the pure transmitted spectrum, especially around the absorption edges which are reduced. He computed the UV and soft X-ray line intensities for a large range of parameters and found that the strongest X-ray lines should have EWs of about $5\text{--}50 \text{ \AA}$. Indeed, George et al. (1998) showed that the introduction of the X-ray emission lines significantly improves the fit of X-ray spectra. Another computation of the emission and reflection spectra has been performed by Krolik & Kriss (1995), in the absence of thermal equilibrium.

The thermal stability of the WA has been discussed by Reynolds & Fabian (1995), using the photoionization code "CLOUDY" (Ferland 1991). They showed the importance of the shape of the ionizing continuum. Also Krolik & Kriss (1995) have studied the thermal stability of the WA.

Since coronal lines are associated with highly ionized ions, the creation of such ions requires a highly powerful process. Two main models could explain the emission of the coronal lines: a hot gas with collisional ionization, with $T > 10^6 \text{ K}$ (Oke & Sargent 1968; Nussbaumer & Osterbrock 1970) and a gas photoionized by a hard UV-X-ray continuum, with $T \sim$ a few 10^4 K (Osterbrock 1969; Grandi 1978; Korista & Ferland 1989, Oliva et al. 1994, Moorwood & Oliva 1991). A third model involving photoionization plus shocks inside the NLR has also been proposed (Viegas-Aldrovandi & Contini 1989).

With a sample of 15 Seyferts (including 11 Seyfert 1s), E97 found that the observed line strengths appear compatible with the predictions of a simple photoionized model calculated by Korista & Ferland (1989) and

Spinoglio & Malkan (1992). The former gave flux ratios of iron coronal lines for very low densities ($n_H \leq 10 \text{ cm}^{-3}$). For PG1211+143, Appenzeller & Wagner (1991) observed a flux ratio of $[\text{Fe VII}] 6087 \text{ \AA} / [\text{Fe X}] 6375 \text{ \AA} = 0.8 \pm 0.2$ compatible with their calculations. The latter made computations for the infrared fine-structure lines for higher densities ($10^2 \leq n_H \leq 10^6 \text{ cm}^{-3}$), and for low ionization parameters (see §3.2 for a definition). Their predictions for $[\text{Mg VIII}]$, $[\text{Si VII}]$, $[\text{Si IX}]$, $[\text{Si X}]$, are referred to the optical forbidden line $[\text{O III}] 5007 \text{ \AA}$ assuming both lines coming from the same medium whereas they are probably produced by two different media. Both articles (Korista & Ferland and Spinoglio & Malkan) used an old version of "CLOUDY" with inaccurate electronic collision strengths for iron ions (Mason 1975): resonance effects near the threshold energy, which have a significant influence on the coronal line fluxes, are not included. These resonance effects are discussed in Dumont & Porquet (1998, hereafter referred as DP98). For example, the electronic collision rates published by Storey et al. (1996) and Pelan & Berrington (1995) (as used in our code for $[\text{Fe XIV}]$ and $[\text{Fe X}]$ respectively) are much larger than the previous data, especially at low temperatures.

3.2. Our model

Our calculations are based on a new code IRIS, which computes detailed multi-wavelength spectra of photoionized and/or collisionally ionized gas, using as input the thermal and ionization structure computed by the photoionization code PEGAS (for more information about these two codes see DP98). It includes a large number of levels and splits the multiplets, thus providing an accurate spectrum from the soft X-rays to the infrared.

All important atomic processes were taken into account: collisional electronic excitation and ionization, three-body recombination, photoionization, radiative and dielectronic recombination, excitation-autoionization and proton impact excitation. Charge transfer has not been implemented for the ground transitions of the coronal ions, since it is negligible in our calculations.

For $[\text{Fe X}]$, the effective electronic collision strengths are taken from Pelan & Berrington (1995) and the proton collision rates from Bely & Faucher (1970). For $[\text{Fe XI}]$ there are no published data available for ground transition effective collision strengths, taking into account the resonance effects, so we have computed them with an IDL subroutine of the CHIANTI database (Dere et al. 1997). The proton collision rates for $[\text{Fe XI}]$ are from Landman (1980). For $[\text{Fe XIV}]$, the effective collision strengths are from Storey et al. (1996) and the proton collision rates for ground level transitions are from Heil et al. (1983).

The element abundances are from Allen (1973).

Our model assumes optically thin clouds in plane-parallel geometry with constant hydrogen density, in ion-

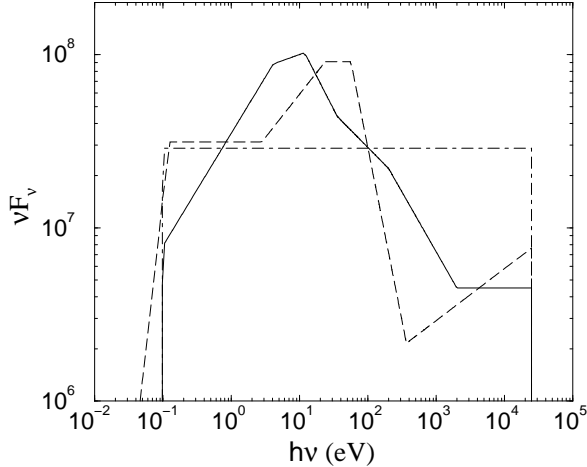


Fig. 6. Shape of the two incident continua for Radio-Quiet quasars used in this paper, as well as a power law continuum ($F_\nu \propto \nu^{-1}$) used for comparison. All continua are normalized at the same ξ . *Solid line*: Laor et al. (1997) (“Laor continuum”), *dashed line*: Mathews & Ferland (1987) but with a break at $10\mu\text{m}$ (“AGN continuum”) and *dot-dashed line*: simple power law.

ization equilibrium and surrounding a central source of radiation. The grid of parameters investigated here is:

1. Hydrogen density: $10^8 \leq n_H \leq 10^{12} \text{ cm}^{-3}$
2. Hydrogen column density: $10^{20} \leq N_H \leq 5 \cdot 10^{23} \text{ cm}^{-2}$
3. Ionization parameter: $2 \leq \xi \leq 4000 \text{ erg cm s}^{-1}$

with $\xi = \frac{L}{n_H R^2}$ where L is the bolometric luminosity (erg.s^{-1}) integrated over 0.1 eV to 100 keV and R is the distance from the ionizing radiation source at the illuminated face of the cloud (cm).

The WA is seen in about 50% of Seyfert 1s, so we suppose that it is present in all these galaxies with a covering factor of 0.5.

Finally, we assume that no dust near the BLR could survive so close to the ionizing central radiation.

We also compute an hybrid model which consists in a photoionized gas out of thermal equilibrium (contrary to the pure photoionized gas). In this case the temperature is set constant at 10^6K .

We use two typical incident continua for Radio-Quiet AGN which are displayed on Figure 6. The first one is published by Laor et al. (1997) (“Laor continuum”), and the second one is used in “CLOUDY” (version 9004, Ferland et al. 1998) and is similar to that published by Mathews & Ferland (1987) but with a sub-millimeter break at $10\mu\text{m}$ (“AGN continuum”). The “Laor continuum” in the X-ray range is based on ROSAT PSPC observations from the Bright Quasar Survey, with high S/N spectra. The selection of the objects in the sample is independent of their X-ray properties to avoid any bias. They found that

the soft X-ray flux at $\sim 0.2\text{--}1 \text{ keV}$ in Mathews & Ferland (1987) is significantly underestimated.

The thermal stability of clouds irradiated by both continua will be discussed in DP98.

Emission due to radiative recombination is shaped as an exponential decay ($\propto \exp(\frac{-(h\nu-x)}{kT})$) with a width of kT and either appears as a hump or fills the absorption hollow near the ionization threshold and could be observed as a blueshift of the edge. In the case of photoionized models, kT is small and the O VII or O VIII edges appear generally smoothed, while in the hybrid models (photoionized gas out of thermal equilibrium with a constant temperature $T=10^6\text{K}$), the hollow can be partly filled. Therefore, our comparisons with observations take into account this emission and the current spectral resolution of the X-ray spectra (ASCA).

The EWs are calculated relatively to the attenuated (transmitted plus emitted) central continuum. The reflected continuum is small and has very little influence on the value of the EWs.

4. Results for the mean observed Seyfert 1 features

Figures 7, 8, 9 and 10 display, in the plane (ξ, N_H) , isovalue curves corresponding to the **mean** observed values of EWs and optical depths, in the case of the pure photoionized and hybrid models and for the “Laor” and “AGN” incident continua ($n_H=10^8\text{--}10^9\text{--}10^{10}\text{--}10^{12}\text{cm}^{-3}$). The thick long dashed, and the upper and lower solid curves represent $\tau_{\text{O VIII}}=0.20$ and $\tau_{\text{O VII}}=0.33$ and 0.10, respectively. $\tau_{\text{O VII}}=0.33$ and $\tau_{\text{O VIII}}=0.20$ are the mean values for Seyfert 1s (see §2.1). $\tau_{\text{O VII}}=0.10$ is roughly the lower limit to detect the presence of the WA. EWs of coronal lines ([Fe X] and [Fe XIV]) and resonance lines (Ne VIII and O VI) are also reported. They are mean values of EWs, except for [Fe XIV] as explained in Sect. 2.2. Grey thin long dashed, lower and upper dotted, dot-dashed and solid curves display isovalues of $\text{EW}([\text{Fe X}])=1.5 \text{ \AA}$, $\text{EW}([\text{Fe XIV}])=2$ and 3 \AA , $\text{EW}(\text{Ne VIII})=4 \text{ \AA}$ and $\text{EW}(\text{O VI})=7 \text{ \AA}$ respectively.

Isovalue curves for the IR coronal lines (upper limits taken at 10 \AA) and the [Fe XI] coronal line (mean value of 4 \AA , based on three objects) are not displayed, since they do not constrain models more than the iron coronal lines [Fe X] and [Fe XIV] and than the resonance lines of Ne VIII and O VI.

For a given incident continuum shape and a given model (pure photoionized or hybrid), only a restricted range of ξ and N_H values is allowed to reproduce both $\tau_{\text{O VII}}=0.33$ and $\tau_{\text{O VIII}}=0.20$. To avoid such a fine-tuning ($\xi \sim 250$ and $N_H \sim 10^{22} \text{ cm}^{-2}$ for the pure photoionized model with the “Laor continuum”), a two-zone warm absorber is suggested, with the O VII edge being formed in a

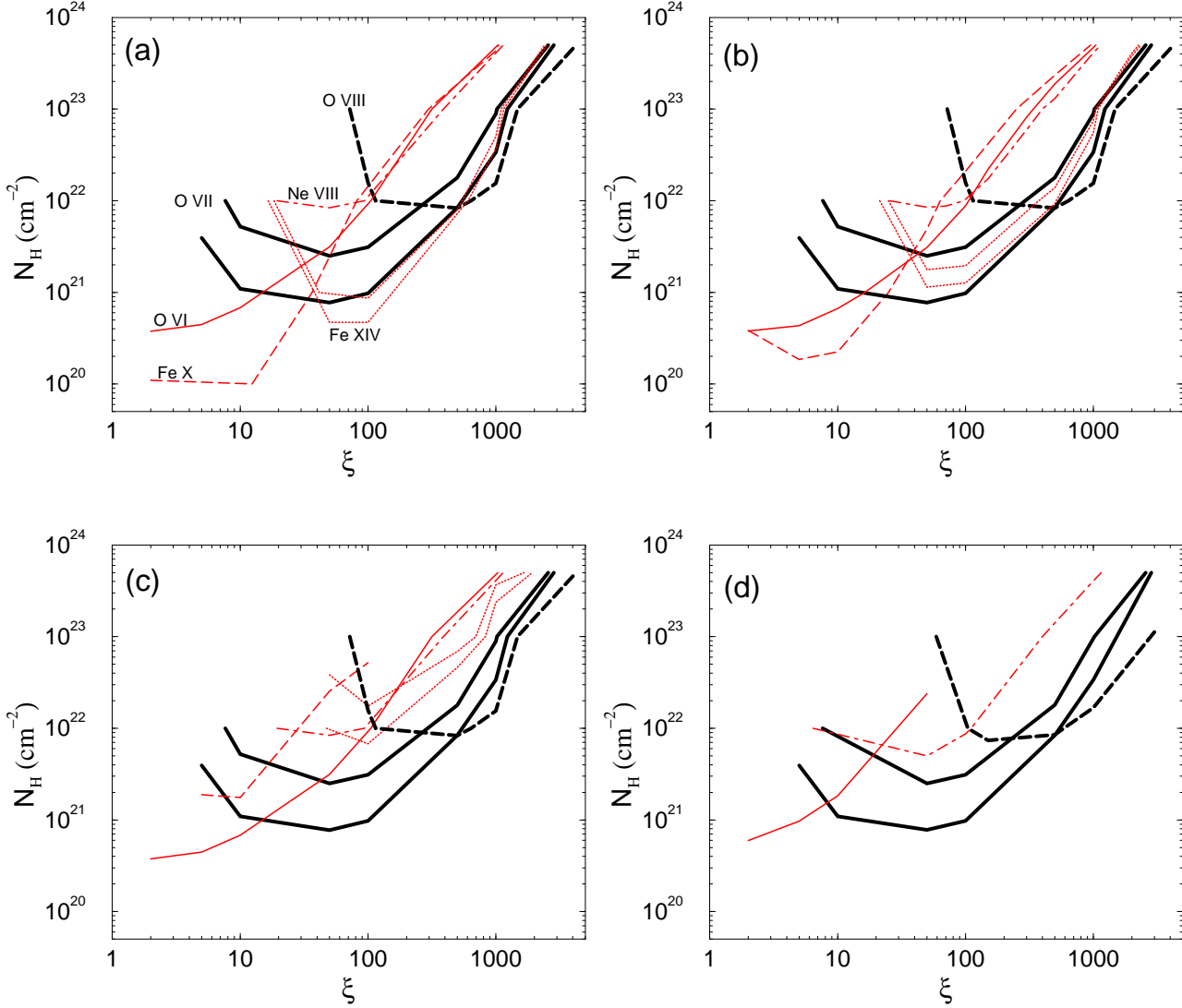


Fig. 7. Isovalue curves in the plane (ξ, N_H) for the pure photoionized model with the incident “Laor continuum” for various hydrogen densities. (a) $n_H = 10^8 \text{ cm}^{-3}$, (b) $n_H = 10^9 \text{ cm}^{-3}$, (c) $n_H = 10^{10} \text{ cm}^{-3}$ and (d) $n_H = 10^{12} \text{ cm}^{-3}$. *Thick lower and upper solid lines:* $\tau_{\text{O VII}}=0.10$ and 0.33 respectively, *thick long dashed line:* $\tau_{\text{O VIII}}=0.20$. *Thin long dashed line:* $\text{EW}([\text{Fe X}])=1.5 \text{ \AA}$, *Thin lower and upper dotted lines* $\text{EW}([\text{Fe XIV}])=2$ and 3 \AA respectively, *thin dotted-dashed line:* $\text{EW}(\text{Ne VIII})=4 \text{ \AA}$ and *thin solid line:* $\text{EW}(\text{O VI})=7 \text{ \AA}$. **For the mean observed Seyfert 1 features, the regions above each thin curve are forbidden since producing too large EWs.**

region at lower ξ and N_H than the O VIII edge. Each zone responsible of a given edge has a negligible contribution to the other edge mainly formed in the second zone.

The regions of parameters (ξ, N_H) above the thin isovalue curves produce EWs for coronal and resonance lines greater than the mean observed values (except for [Fe XIV] as explained above). Therefore, **the region above each thin curve is forbidden.**

4.1. Pure photoionized models

Figure 7 shows the isovalue curves for the incident “Laor continuum”. As an example, results for each density are

displayed in Table 1. For $\tau_{\text{O VII}}=0.33$, a high density ($n_H \geq 10^{10} \text{ cm}^{-3}$) is required, in order not to produce larger EWs of [Fe X] or [Fe XIV] than the mean observed ones. A very small region where $\tau_{\text{O VIII}}=0.20$ could correspond to $n_H=10^8 \text{ cm}^{-3}$ if $N_H \geq 10^{22} \text{ cm}^{-2}$ and $\xi \geq 600$.

Figure 8 shows the isovalue curves for the case of the incident “AGN continuum”. A one-zone model requires $\xi \sim 500$ and $N_H \sim 7 \cdot 10^{21} \text{ cm}^{-2}$. For $\tau_{\text{O VII}}=0.33$, a high density is required ($n_H > 10^9 \text{ cm}^{-3}$). For $\tau_{\text{O VIII}}=0.20$, n_H values as low as 10^9 cm^{-3} are allowed.

Table 1. Results for the pure photoionized model with the incident “Laor continuum” for the mean observed Seyfert 1 features (cf Fig. 7).

n_H (cm^{-3})	O VII zone $\tau_{\text{O VII}}=0.33$ ($\xi < 250$)	O VIII zone $\tau_{\text{O VIII}}=0.20$ ($\xi > 250$)
10^8	EW([Fe x]) $\gg 1.5\text{\AA}$ or EW([Fe xiv]) $\gg 3\text{\AA}$ \implies this density is ruled out	<ul style="list-style-type: none"> • if ($\xi \leq 600$) then EW([Fe xiv])$\gg 3\text{\AA}$ • else no constraint
10^9	idem as for $n_H=10^8\text{cm}^{-3}$	idem as for $n_H=10^8\text{cm}^{-3}$
10^{10}	<ul style="list-style-type: none"> • if ($\xi \leq 40$) then EW(O vi)$\gg 7\text{\AA}$ • else no constraint 	no constraint
10^{12}	<ul style="list-style-type: none"> • if ($\xi \leq 20$) then EW(O vi)$\gg 7\text{\AA}$ • else no constraint 	no constraint

4.2. Results for the hybrid models

The pure photoionized model might be too simple to represent the WA, e.g. it could be in non-equilibrium or collisionally photoionized. So we have computed a grid for an hybrid model consisting in a photoionized gas out of thermal equilibrium, the temperature being taken constant at $T_e = 10^6$ K. This temperature corresponds approximatively to the maximum of the ionic abundance of Fe X and Fe XI ions.

Figure 9 shows the isovalue curves for the incident “Laor continuum”. Both edges could be produced in the same region for $\xi \sim 200$ and $N_H \sim 5 \cdot 10^{22} \text{cm}^{-2}$. For $\tau_{\text{O VII}}=0.33$, in order to have a non negligible allowed region, $n_H > 10^{10}\text{cm}^{-3}$ is required with $50 < \xi < 200$ and $10^{22} < N_H < 5 \cdot 10^{22} \text{cm}^{-2}$. $\tau_{\text{O VIII}}=0.20$ could be accounted for by densities as low as $n_H \sim 10^8\text{cm}^{-3}$ if $N_H \geq 4 \cdot 10^{22}\text{cm}^{-2}$ and $\xi \geq 500$.

Figure 10 displays the corresponding isovalue curves for the incident “AGN continuum”. The one-zone model requires $\xi \sim 500$ and $N_H \sim 3.5 \cdot 10^{22} \text{cm}^{-2}$. For $\tau_{\text{O VII}}=0.33$, a high density is required ($n_H \geq 10^{10} \text{cm}^{-3}$) as in the previous cases. For $\tau_{\text{O VIII}}=0.20$, high ionization parameters ($\xi > 100$) are required for low density values ($n_H \sim 10^8 \text{cm}^{-3}$).

4.3. Conclusions for the pure photoionized and for the hybrid models

The confrontation of the regions of parameters (ξ, N_H) allowed by the EWs with those producing $\tau_{\text{O VII}}$ and $\tau_{\text{O VIII}}$ separately, strongly constrains the hydrogen density of the WA. For $n_H \leq 10^{10} \text{cm}^{-3}$ the physical parameters are mainly constrained by the coronal lines due to their weak

observed EWs and their high critical densities. On the contrary, at higher densities constraints are given by the resonance lines.

The isovalue curves between the models with the “Laor” and “AGN” continua are shifted by a factor of about 2 in ξ due to continuum shape differences. In the same way, similar values of the optical depths for the hybrid case are obtained for a ξ value five times smaller than for the pure photoionized case. Notice that for the hybrid model, the Ne VIII line is enhanced.

A one-zone model which would be responsible for all features considered here is ruled out by all considered models.

For both pure photoionized and hybrid models a high density $n_H \geq 10^{10}\text{cm}^{-3}$ for the WA is required for $\tau_{\text{O VII}}=0.33$, in order to explain the mean observed coronal lines and resonance lines of Seyfert 1 galaxies. On the contrary, $\tau_{\text{O VIII}}=0.20$ could be obtained with n_H as low as 10^8cm^{-3} but for a smaller range of parameters corresponding to high ξ and N_H values.

5. Example of a particular case: MCG-6-30-15

It is interesting to apply our computations to the Seyfert 1 galaxy MCG-6-30-15, for which several emission lines have been measured, as well as the optical depths of the O VII and O VIII edges.

With ASCA, Reynolds et al. (1995) observed in this object that the optical depth at the O VIII edge ($\tau_{\text{O VIII}}$) responds to continuum changes with a characteristic time-scale of about 10^4s , whereas the optical depth of O VII ($\tau_{\text{O VII}}$) seems to be almost constant during all the observations. Otani et al. (1996) made the hypothesis that the WA could consist of two different components: the

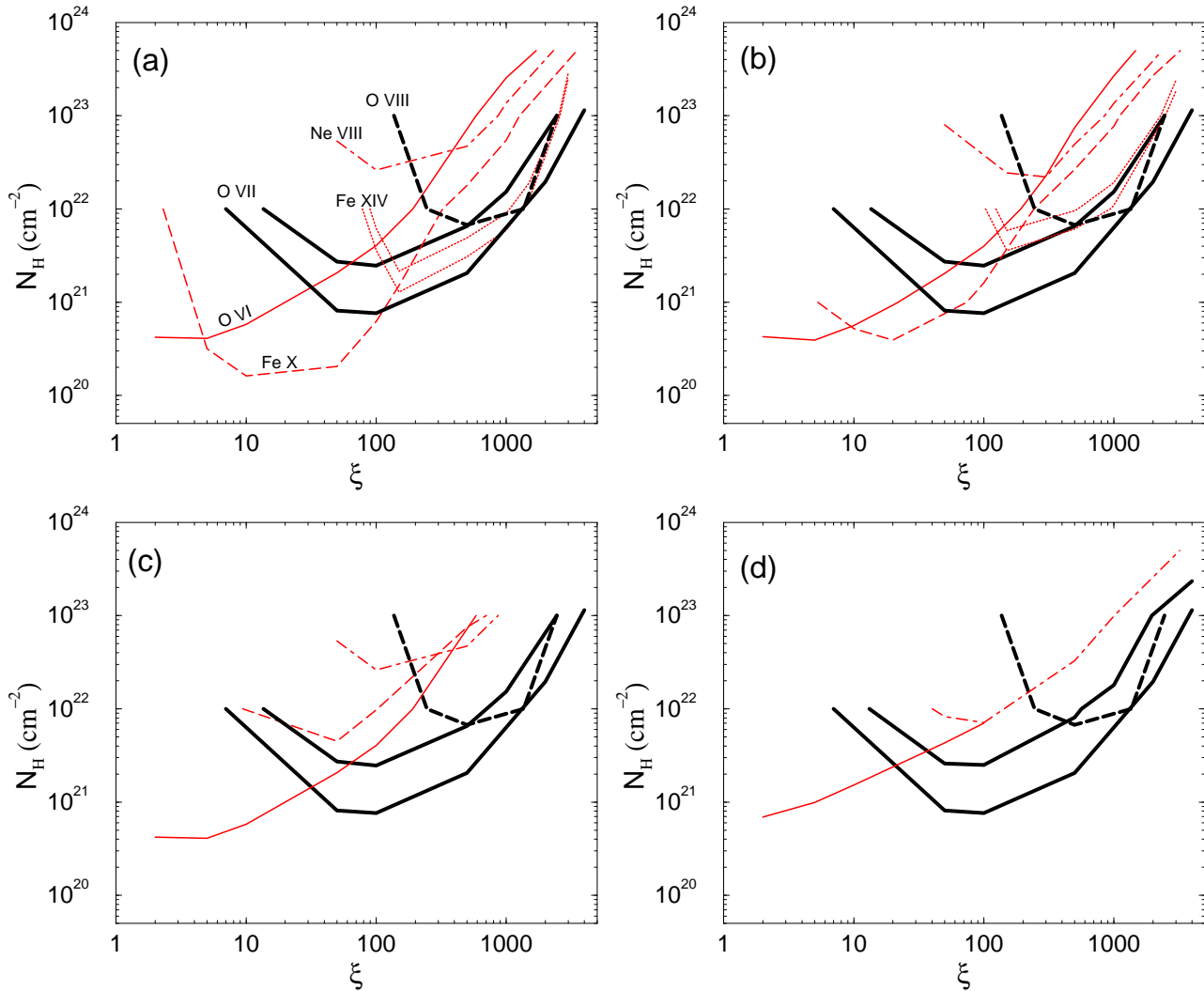


Fig. 8. Same as Fig. 7 for the pure photoionized model with the “AGN continuum”.

inner absorber which has a high ionization, responsible in large part of the O VIII edge and located in or just outside the BLR ($R < 10^{17}$ cm), and the outer absorber mainly responsible of the O VII edge, less ionized, and located near the molecular torus ($R > 1$ pc). With BeppoSax data, Orr et al. (1997) confirmed that $\tau_{\text{O VII}}$ did not change significantly during the exposure time (~ 400 ks), contrary to $\tau_{\text{O VIII}}$. But they did not find any simple correlation between $\tau_{\text{O VIII}}$ and the continuum luminosity, although the variations of the continuum emission and those of the WA (edges) have a similar time-scale ($< 2 \cdot 10^4$ s). The ASCA mean spectrum obtained in July 1994 (Otani et al. 1996) and the BeppoSax spectrum (Orr et al. 1997) give optical depth values consistent with those derived from the 1993 ASCA data (Reynolds et al. 1995). In the following we use the two sets of values derived by Reynolds et al.: $\tau_{\text{O VII}} = 0.53 \pm 0.04$, 0.63 ± 0.05 and $\tau_{\text{O VIII}} = 0.19 \pm 0.03$, 0.44 ± 0.04 , respectively for the July and August 1993 datasets.

Data for the EWs of iron coronal lines are taken from Reynolds et al. (1997). They gave $\text{EW}([\text{Fe X}]) = 3.0 \pm 0.4 \text{ \AA}$, $\text{EW}([\text{Fe XI}]) = 3.0 \pm 0.7 \text{ \AA}$ and $\text{EW}([\text{Fe XIV}]) = 5.2 \pm 0.4 \text{ \AA}$. But the EW measurements of [Fe X] and [Fe XI] have not been galaxy-subtracted, they are therefore underestimated. Since no information is given to estimate the contribution of the stellar component near these lines, we take EWs for [Fe X] and [Fe XI] of 4 \AA , estimating the effect of a dilution of about 1/3. This value is close to that found by Serote-Roos et al. (1996) for NGC 3516 which displays an EW of the Calcium triplet about equal to that of MCG-6-30-15 (Morris & Ward 1988). The [Fe XIV] 5303 Å line is blended with [Ca V] 5309 Å, so its EW is overestimated. That is why we also use another EW value for [Fe XIV] of 3 \AA which should be closer to the real value.

In Figs. 11, 12, 13 and 14 both values obtained by Reynolds et al. (1995) for each optical depth are displayed ($\tau_{\text{O VII}} = 0.53$ and 0.63 : thick lower and upper solid lines re-

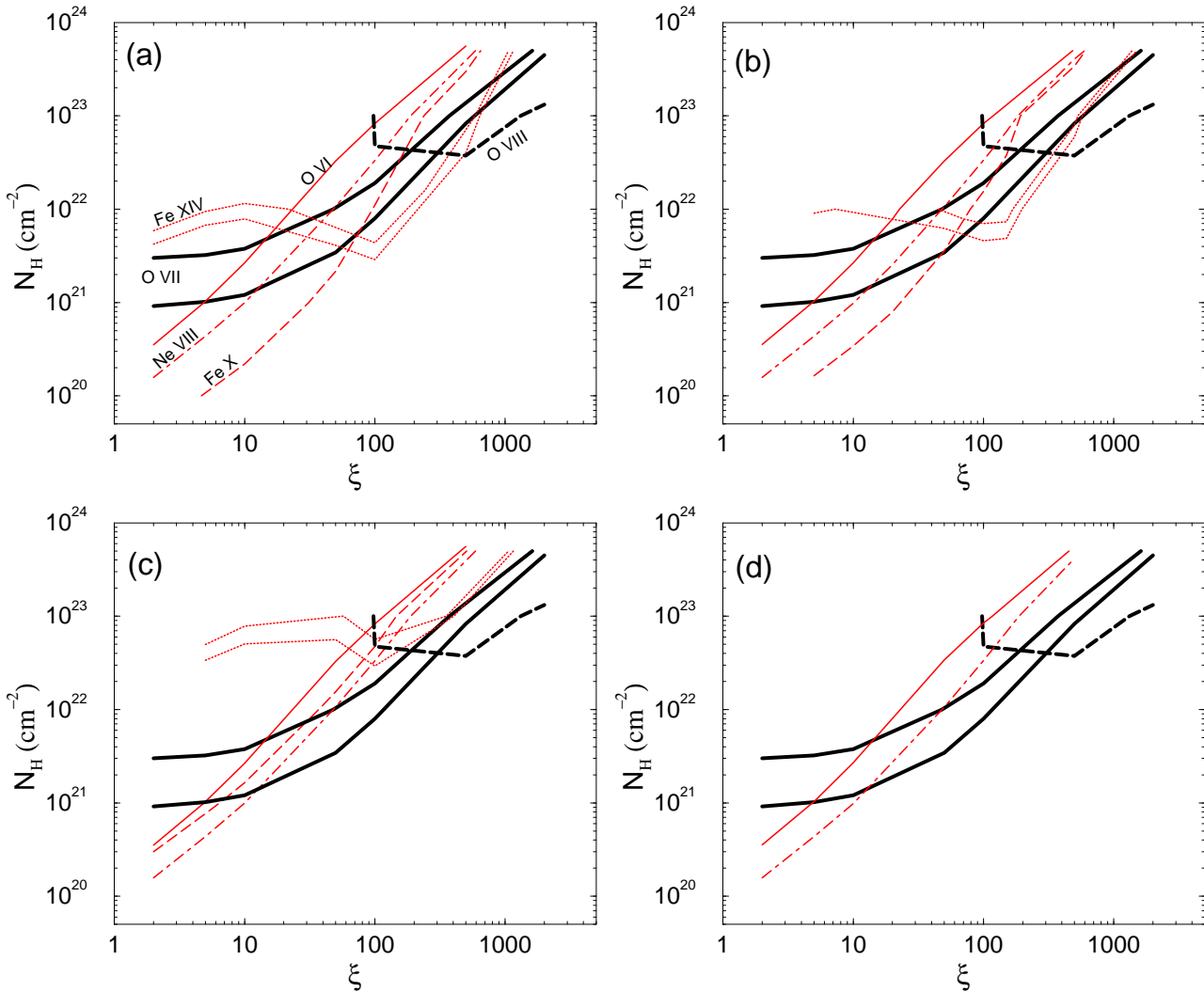


Fig. 9. Same as Fig. 7 for the hybrid model with the “Laor continuum”.

spectively and $\tau_{\text{O VIII}}=0.19$ and 0.44 : thick lower and upper long dashed lines respectively). Isovalue curves for the optical iron coronal lines are also reported (thin lower and upper long dashed lines: $\text{EW}([\text{Fe X}])=3$ and 4 \AA , thin lower and upper dot-dashed lines: $\text{EW}([\text{Fe XI}])=3$ and 4 \AA , thin lower and upper solid lines: $\text{EW}([\text{Fe XIV}])=3$ and 5 \AA respectively).

In order to reproduce both $\tau_{\text{O VII}}$ and $\tau_{\text{O VIII}}$ values of July 1993 (one-zone model), an ionization parameter of the order of 200–400 is needed depending on the shape of the ionized spectrum and of the type of model (pure photoionized or hybrid). A range of ξ between 300 to 900 is required for the August 1993 data. These values are significantly greater than values found by Reynolds et al. (1995), reflecting the different shape of the ionization continuum (power law) they assumed. The ratio of the ionization parameter values which are derived for both epochs allows to get rid of the shape of the ionizing continuum. This ratio is consistent with the one obtained by Reynolds et al.

(~ 1.3) except for the pure photoionized model with the “AGN continuum” (~ 2.6).

However, the short variability time-scale ($\sim 10\,000 \text{ s}$) of the O VIII edge favors a two-zone model (Reynolds et al. 1995, Otani et al. 1996).

For the pure photoionization model with the “AGN continuum” a n_{H} value of about 10^9 cm^{-3} could account for the $[\text{Fe XIV}]$ ($\text{EW} \sim 3 \text{ \AA}$) for a narrow range of ξ : 150–300 (cf Fig. 12).

For the range of densities considered here, the inner zone responsible of the O VIII edge would contribute weakly to the coronal lines of Fe X and Fe XI and it is not constrained by the $[\text{Fe XIV}]$ line at very high values of ξ .

The recombination time-scale derived for the high density value associated with the O VII edge is much smaller than the variability time-scale of the associated region. Thus, the photoionization equilibrium can be applied.

We also point out that our computations are restricted to dust-free models, whereas dust inside the outer warm

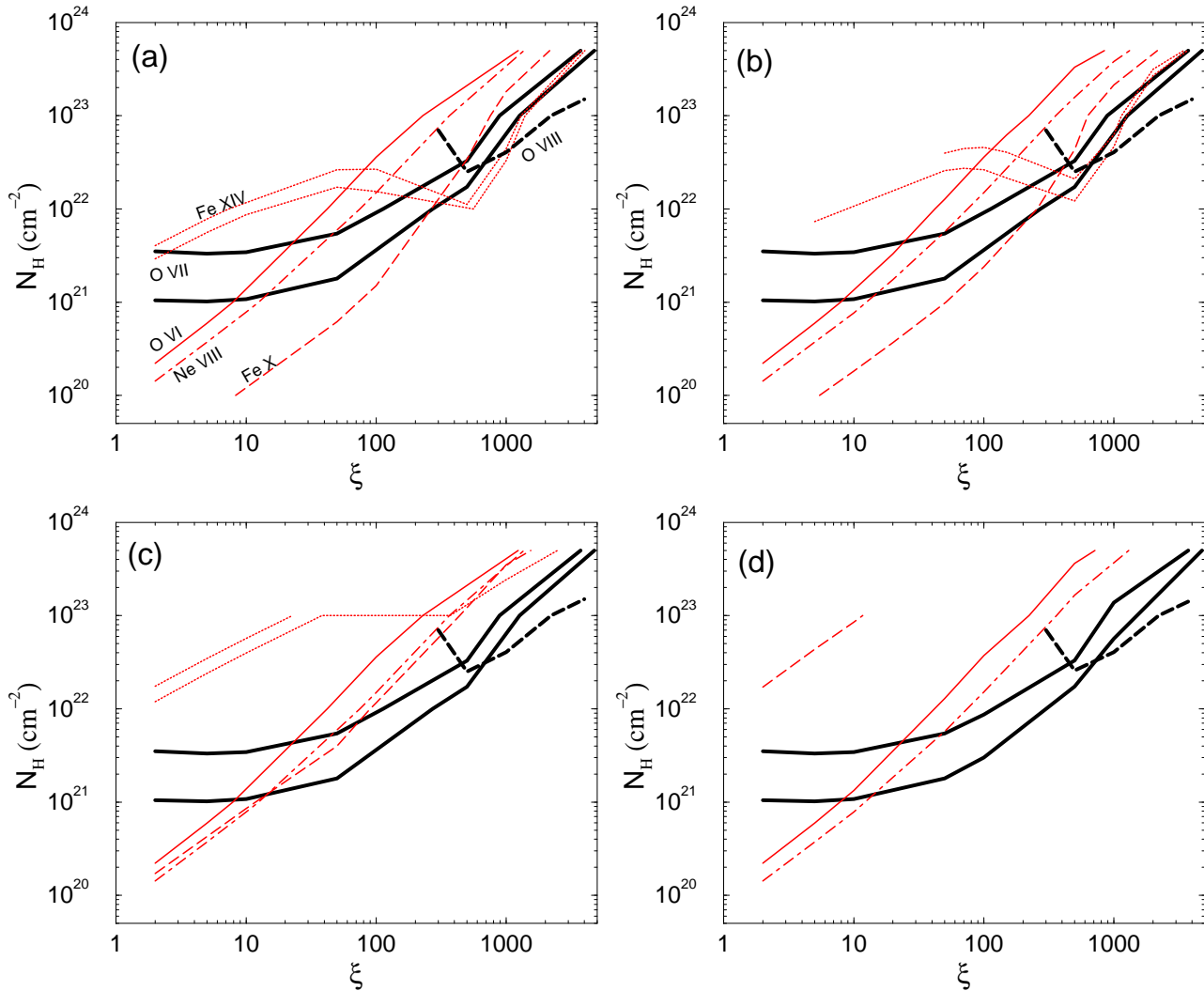


Fig. 10. Same as Fig. 7 for the hybrid model with the “AGN continuum”.

absorber has been considered as a viable solution by Reynolds et al. (1997).

6. Conclusions

Using a photoionization code, including the most recent atomic data available for the coronal lines, we have found that the coronal lines could be formed in the Warm Absorber of the Seyfert 1 galaxies, and they strongly constrain its physical parameters, especially the hydrogen density. In order to take into account the available observational constraints, a high density is required for the mean observed Seyfert 1 features, as well as for the case of MCG-6-30-15, for both considered models (photoionized medium in or out of thermal equilibrium). A model with two different regions is favored, an inner zone mainly producing the O VIII associated with a high ionization parameter ($\xi \sim$ a few hundreds) and an outer zone where the O VII edge is formed, corresponding to a smaller ξ (\sim a few tens). A density $n_H \sim 10^{10} \text{ cm}^{-3}$ and $\xi \sim 10\text{--}100$ for a typ-

ical Seyfert 1 O VII edge implies a radius similar to that of the BLR ($R \sim$ a few 10^{16} cm). For higher ξ producing the O VIII edge, a region of low density ($\sim 10^8 \text{ cm}^{-3}$) is not obviously ruled out, which would be at a similar distance as the BLR, while a more likely high density region ($\sim 10^{10} \text{ cm}^{-3}$) would be located even inside the BLR.

The gas pressure being proportional to the ratio of the temperature over the ionization parameter ($P_{gas} \propto T/\xi$), we deduce that the pressure is the same in the BLR and in the WA (using $T_{BLR} \sim 10^4 \text{ K}$ and $\xi_{BLR} \sim 10$, $T_{WA} \sim 10^5 \text{ K}$ and $\xi_{WA} \sim 100$). So the WA could coexist with the BLR and be a second gaseous phase of this medium.

In this paper, several assumptions such as a solar abundance, a constant density, a covering factor of 0.5 and a dust-free medium have been made. This analysis is restricted to available coronal and high-ionization resonance line measurements. In a near future additional constraints will be brought by measurements of coronal lines in the IR and of X-ray resonance lines which will be detectable

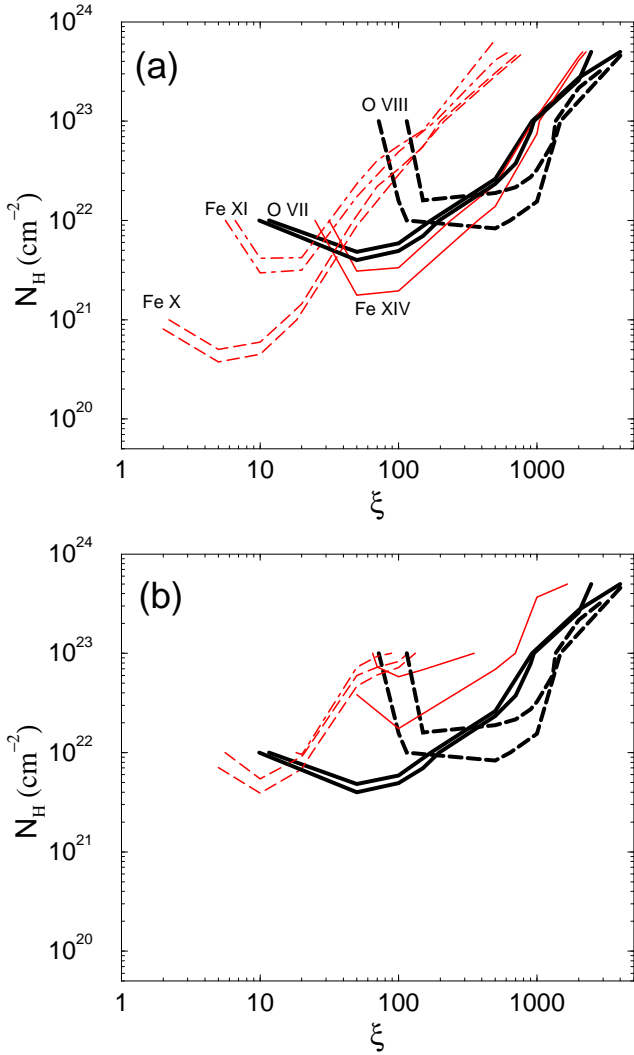


Fig. 11. Isovalue curves for MCG-6-30-15 for the pure photoionized model with the “Laor continuum” for two different hydrogen densities: (a) $n_H=10^9 \text{ cm}^{-3}$ and (b) $n_H=10^{10} \text{ cm}^{-3}$. *Thick lower and upper solid lines:* $\tau_{\text{O VII}}=0.53$ and 0.63 respectively, *thick lower and upper dashed lines:* $\tau_{\text{O VIII}}=0.19$ and 0.44 , *thin lower and upper long dashed lines:* $\text{EW}([\text{Fe X}])=3$ and 4 \AA , *thin lower and upper dot-dashed lines:* $\text{EW}([\text{Fe XI}])=3$ and 4 \AA , *thin lower and upper solid lines* $\text{EW}([\text{Fe XIV}])=3$ and 5 \AA respectively.

thanks to the next generation of X-ray telescopes (AXAF, XMM, ASTRO-E). Our knowledge of the WA should also be improved by X-ray temporal variability studies. These investigations are crucial since they provide important diagnostics for the physical conditions which prevail in the ionized plasma. For instance, if the recombination time-scale is larger than the variability time-scale of the source, photoionization equilibrium could not be applied (Reynolds & Fabian 1995).

In the same way the fact that coronal lines could be

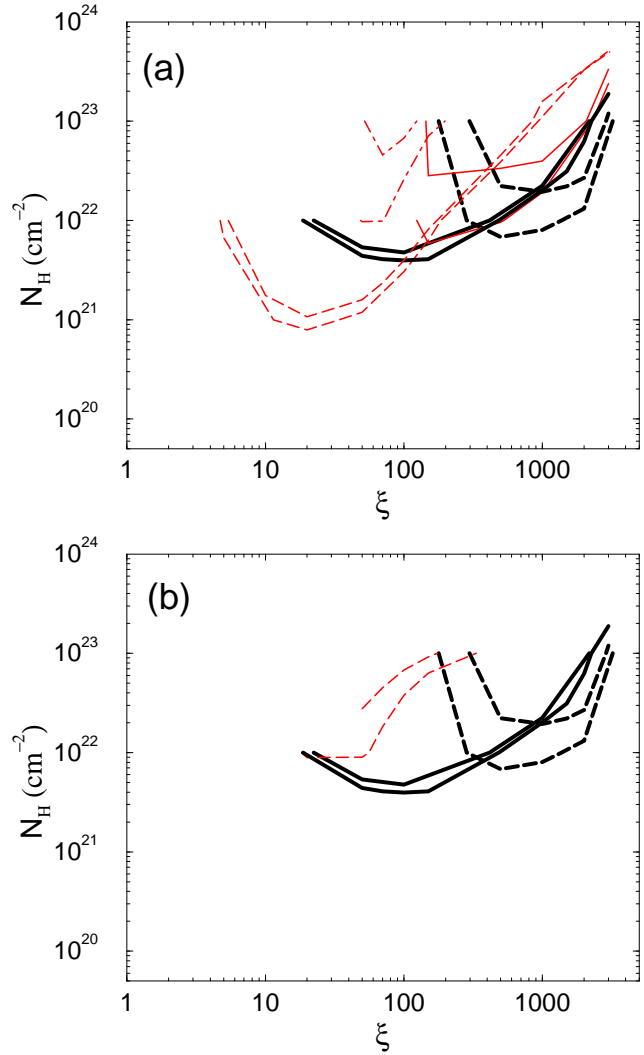


Fig. 12. Same as Fig. 11 for the pure photoionized models with the “AGN continuum”.

formed in the WA should be confirmed by detection of rapid variations of these lines, which have not yet been observed.

Acknowledgements. We acknowledge Monique Joly for fruitful discussions and Claude Zeippen for helpful conversations about atomic processes.

References

- Allen, C. W., 1973, in “Astrophysical quantities”, London: University of London, Athlone Press, 3rd ed., p31
- Appenzeller, I., Wagner, S. J., 1991 *A&A* 250, 57
- Bely, O. & Faucher, P., 1970, *A&A* 6, 88
- Boller, Th., Meurs, E. J. A., Brinkmann, W., et al., 1992, *A&A* 261, 57
- Dere, K. P., Landi, E., Mason, H. E. et al., 1997, *A&AS* 125, 149
- Dumont, A.-M., Porquet, D., 1998, in preparation (DP98)
- Erkens, U., Appenzeller, I., Wagner, S., 1997, *A&A* 323, 707 (E97)

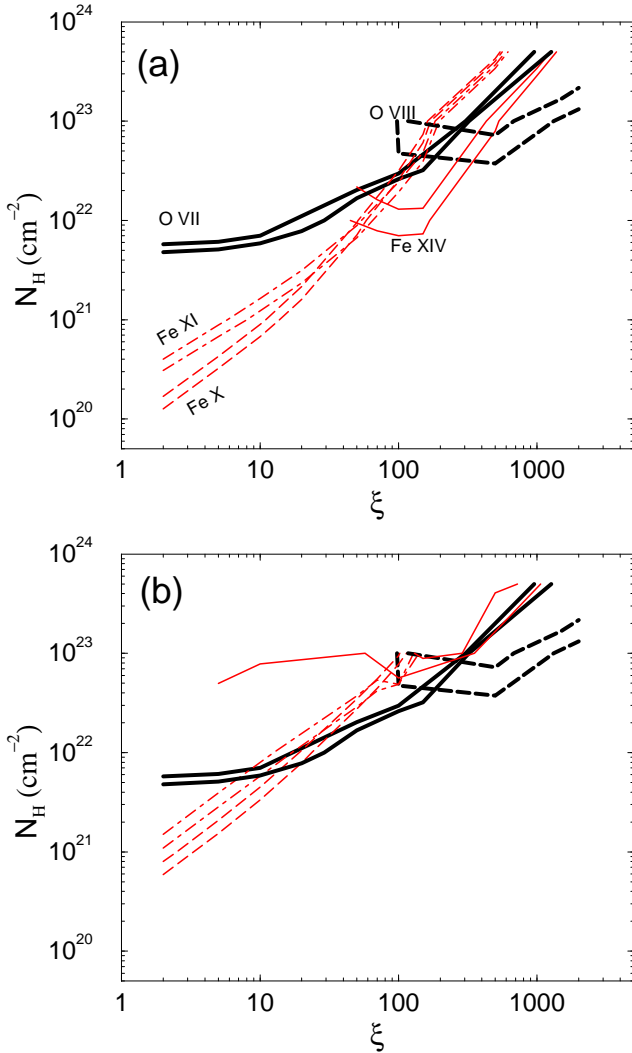


Fig. 13. Same as Fig. 11 for the hybrid models with the “Laor continuum”.

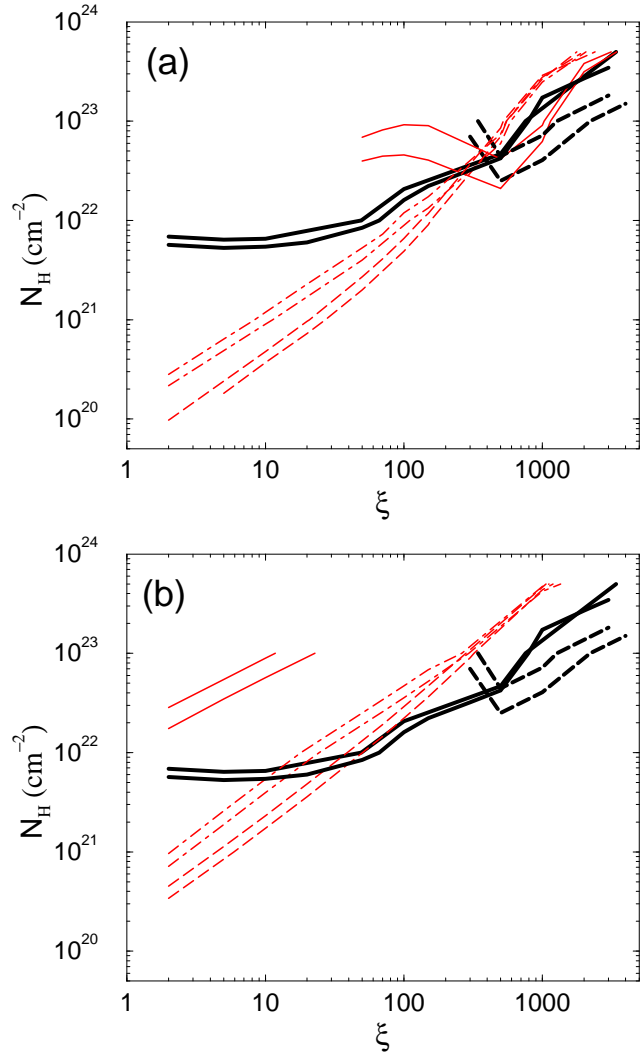


Fig. 14. Same as Fig. 11 for the hybrid models with the “AGN continuum”.

Feigelson, E. D., Nelson, P. I., 1985, *ApJ* 293, 192
 Ferland, G. J. 1991, Ohio State University, Astronomy Department Internal Report 91-01
 Ferland, G. J., Korista, K. T., Verner, D. A. et al., 1998, *PASP* 110, 761
 Genzel, R., Weitzel, L., Tacconi-Garman, L. E. et al., 1995, *ApJ* 444, 129
 George, I. M., Turner, T. J., Netzer, H., 1995, *ApJ* 438, L67
 George, I. M., Turner, T. J., Netzer, H. et al., 1998, *ApJS* 114, 73
 Giannuzzo, E., Rieke, G. H., Rieke, M. J., 1995, *ApJ* 446, L5
 Grandi, S. A., 1978, *ApJ* 221, 501
 Guainazzi, M., Mihara, T., Otani, C., Matsuoka, M., 1996, *PASJ* 48, 781
 Halpern, J. C., 1984, *ApJ* 281, 90
 Hamann, F., Shields, J. C., Ferland, G. J., Korista, K. T., 1995, *ApJ* 454, 688
 Heil, T. G., Kirby, K., Dalgarno, A., 1983, *Phys. Rev. A* 27, 2826
 Korista, K. T., Ferland, G. J., 1989, *ApJ* 343, 678
 Krolik, J. H., Kriss, G. A., 1995, *ApJ* 447, 512

Landman, D. A., 1980, *ApJ* 240, 709
 Laor, A., Fiore, F., Elvis, M. et al., 1997, *ApJ* 477, 93
 Lavalley, M., Isobe, T., Feigelson, E., 1992 in “Astronomical Data Analysis Software and Systems I”, A.S.P. Conference Series Vol. 25, Diana M. Worrall, Chris Biemesderfer, and Jeannette Barnes, eds., p. 245.
 Mason, H. E., 1975, *MNRAS* 170, 651
 Mathews, W. G. & Ferland, G.J., 1987 *ApJ* 323, 456
 Mihara, T., Matsuoka, M., Mushotzky, R. F. et al., 1994, *PASJ* 446, L137
 Moorwood, A. F. M., Oliva, E., 1991, *The Messenger* 63, 57
 Morris, S. L., Ward, M. J., 1988, *MNRAS* 230, 639
 Nandra, K., Pounds, K. A., 1994, *MNRAS* 268, 405
 Netzer, H., 1993, *ApJ* 411, 594
 Netzer, H., 1996, *ApJ* 473, 781
 Nussbaumer, H., & Osterbrock, D.E., 1970, *ApJ* 161, 811
 Oke, S., Sargent, W., 1968, *ApJ* 151, 807
 Oliva, E., Salvati, M., Moorwood, A. F. M., Marconi, A., 1994, *A&A* 288, 457
 Orr, A., Molendi, S., Fiore, F. et al., 1997, *A&A* 324, L77
 Osterbrock, D. E., 1969, *Astrophys. Letters* 4, 57

- Otani, C., Kii, T., Reynolds, C. S. et al., 1996, PASJ 48, 211
- Pelan J., Berrington, K. A., 1995, *A&A* 110, 209
- Penston, M. V., Fosbury, R. A. E., Boksenberg, A. et al., 1984, MNRAS 208, 347
- Piro, L., Balucinska-Church, M., Fink, H. et al., 1997, *A&A* 319, 74
- Porquet, D., Dumont, A.-M., 1998, in "Structure and Kinematics of Quasar Broad Line Regions", Eds C. M. Gaskell, W. N. Brandt, M. Dietrich, D. Dultzin-Hacyan, and M. Eracleous, ASP Conf. Ser., in press
- Reynolds, C. S., 1997, MNRAS 286, 513
- Reynolds, C. S., Fabian, A. C., 1995, MNRAS 273, 1167
- Reynolds, C. S., Fabian, A. C., Nandra, K. et al., 1995, MNRAS 277, 901
- Reynolds, C. S., Ward, M. J., Fabian, A. C., Celotti, A., 1997, MNRAS 291, 403
- Rush, B., Malkan, M. A., Fink, H. H., Voges, W., 1996, ApJ 471, 190
- Schartel, N., Schmidt, M., Fink, H. H. et al., 1997, *A&A* 320, 696
- Serote-Roos, M., Boisson, C., Joly, M., Ward, M. J., 1996, MNRAS 278, 897
- Shields, J. C., Ferland, G. J., Peterson, B.M., 1995, ApJ 441, 507
- Spinoglio, L., Malkan, M.A., 1992, ApJ 399, 504
- Storey, P. J., Mason, H. E., Saraph, H. E., 1996, *A&A* 309, 677
- Thompson, R.I., 1996, ApJ 459, L61
- Viegas-Aldrovandi, S. M., Contini, M., 1989, *A&A* 215, 253
- Zheng, W., Kriss, G. A., Davidsen, A. F., 1995, ApJ 440, 606
- Zheng, W., Kriss, G. A., Telfer, R. C. et al., 1997, ApJ 475, 469